AIP | Review of Scientific Instruments

Invited Article: Autonomous assembly of atomically perfect nanostructures using a scanning tunneling microscope

Robert J. Celotta, Stephen B. Balakirsky, Aaron P. Fein, Frank M. Hess, Gregory M. Rutter, and Joseph A. Stroscio

Citation: Review of Scientific Instruments **85**, 121301 (2014); doi: 10.1063/1.4902536
View online: http://dx.doi.org/10.1063/1.4902536
View Table of Contents: http://scitation.aip.org/content/aip/journal/rsi/85/12?ver=pdfcov
Published by the AIP Publishing

Invited Article: Autonomous assembly of atomically perfect nanostructures using a scanning tunneling microscope

Robert J. Celotta,[1,a)] Stephen B. Balakirsky,[2,3] Aaron P. Fein,[4] Frank M. Hess,[1] Gregory M. Rutter,[1] and Joseph A. Stroscio[1,a)]

[1]*Center for Nanoscale Science and Technology, National Institute of Standards and Technology, Gaithersburg, Maryland 20899, USA*
[2]*Engineering Laboratory, National Institute of Standards and Technology, Gaithersburg, Maryland 20899, USA*
[3]*Georgia Tech Research Institute, Atlanta, Georgia 30332, USA*
[4]*Physical Measurement Laboratory, National Institute of Standards and Technology, Gaithersburg, Maryland 20899, USA*

(Received 8 August 2014; accepted 11 November 2014; published online 17 December 2014)

A major goal of nanotechnology is to develop the capability to arrange matter at will by placing individual atoms at desired locations in a predetermined configuration to build a nanostructure with specific properties or function. The scanning tunneling microscope has demonstrated the ability to arrange the basic building blocks of matter, single atoms, in two-dimensional configurations. An array of various nanostructures has been assembled, which display the quantum mechanics of quantum confined geometries. The level of human interaction needed to physically locate the atom and bring it to the desired location limits this atom assembly technology. Here we report the use of autonomous atom assembly *via* path planning technology; this allows atomically perfect nanostructures to be assembled without the need for human intervention, resulting in precise constructions in shorter times. We demonstrate autonomous assembly by assembling various quantum confinement geometries using atoms and molecules and describe the benefits of this approach. [http://dx.doi.org/10.1063/1.4902536]

TABLE OF CONTENTS

I. INTRODUCTION

The scanning tunneling microscope (STM) and related scanned probe technologies have demonstrated a broad range of measurement capabilities including mapping the local density of electron states, magnetism, and electro-mechanical properties, to name a just few.[1–4] Two of the most significant achievements of the STM have been the manipulation of single atoms and molecules and the building of various nanostructures that display a host of quantum properties.[5–37] This technology allows the human hand to reach into a realm that is 1×10^9 times removed from our macroscopic world and move single atoms.

Atom manipulation with the STM utilizes an interaction we term a tunable chemical bond, which occurs between the atoms at the end of the STM probe tip and a surface adatom.[6] It is tunable because of our ability to control the tip-adatom distance in the STM with picometer precision through the use of piezoelectric actuators.

Two types of manipulation are possible to create nanostructures; lateral and vertical manipulation [Fig. 1]. Lateral manipulation is the predominant method used. It relies on creating a temporary bond between the probe tip atoms and the adatom. Once this bond is established, the atom is moved along the surface to a new location where the bond is broken, allowing the adatom to settle into its new location. A delicate balance between the substrate-adatom bond strength and that of the probe-adatom bond must be established. When such a balance is not readily attainable, researchers have sometimes been able to use vertical manipulation, where the probe-adatom tip bond is strengthened to the point of picking up the adatom from the surface and bonding it solely to the probe

a)Authors to whom correspondence should be addressed. Electronic addresses: robert.celotta@nist.gov and joseph.stroscio@nist.gov

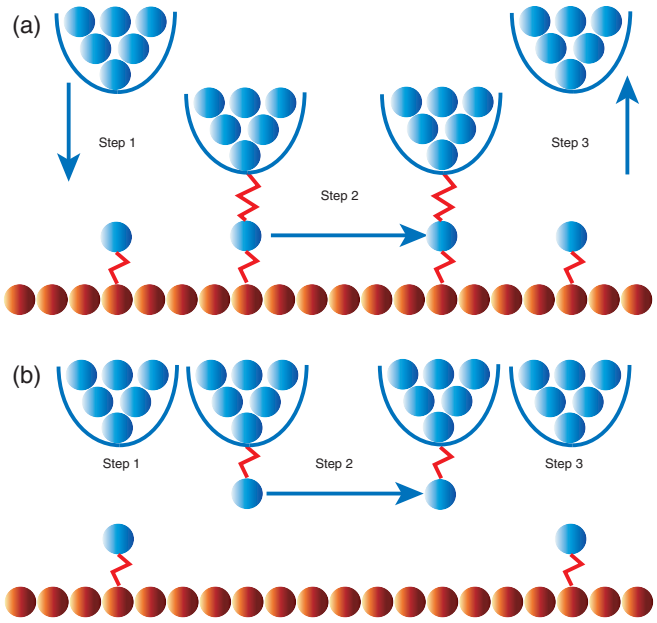

FIG. 1. (a) Schematic of lateral atom manipulation. Step 1, acquire adatom by decreasing tunneling impedance to form a tunable chemical bond. Step 2, move laterally to new location at manipulation impedance keeping adatom trapped under probe tip. Step 3, release adatom by increasing tunneling impedance to the topographic imaging value. (b) Schematic of vertical atom manipulation. Step 1, apply positive voltage pulse to remove adatom from surface and put it on the end of the probe tip. Step 2, move tip to new location. Step 3, apply negative voltage pulse to remove adatom from the tip and deposit it on the surface.

tip. The tip is then positioned to a new location, and the process is reversed, placing the adatom back onto the surface in a new location. Vertical manipulation is less reliable than lateral manipulation, but simple nanostructures have been built which have enabled exquisite experiments on, for example, quantum magnetic interactions in nanostructures.[27,28,32,35]

A variety of interesting nanostructures have been built using atom manipulation, such as quantum corrals[8,16] and operational logic devices.[19,33] The latter[19] represent some of the most elaborate structures that have been built to date, containing over 500 atoms and requiring over 24 h to construct. Even the construction of a simple circular atom corral can prove challenging since the builder must map the desired circular geometry onto a crystal lattice that typically has rectilinear symmetry.

Ultimately, it is desirable to have a system that automatically maps the desired structure onto the available, stable substrate adatom locations taking into account the initial positions of the adatom source material, the interactions between adatom, tip, and substrate, the optimal assembly sequence and path. Such a system would allow the ready construction of atomically perfect, or possibly purposely slightly imperfect,[34] nanostructures whose properties could then be determined. This paper describes the development of just such a device, an Autonomous Atom Assembler (AAA). We describe the implementation of the AAA system, demonstrate its use in the construction of some simple geometric nanostructures, and discuss its limitations and possible future improvements.

II. THE AAA EXPERIMENTAL SYSTEM

The AAA system is comprised of an AAA control computer that plans, controls, and displays the status of the autonomous assembly process; a separate, dedicated STM computer control system; and a custom-built, cryogenic ultra-high vacuum STM [Fig. 2]. The AAA control computer provides high level control commands to the STM control system via Message Passing Interface (MPI) when autonomous assembly of nanostructures is underway. The basic electrical control of the STM is performed by the STM computer via a VXI instrumentation system which provides all necessary electrical signals and performs all data acquisition.

The STM system consists of several interconnected UHV systems for sample and tip preparation in addition to the microscope system housed on top of and inside of a superconducting magnet cryostat [Fig. 3].[38] A circular UHV transfer station located in the middle of the chambers allows samples and tips to be translated among the various UHV systems. Each chamber can be isolated and baked to achieve UHV pressures. A two-stage load lock chamber facilitates introduction of samples and probes from atmosphere. A field-ion microscope is used for tip preparation at room temperature.[38] The STM incorporates a novel modular STM head [Figs. 4 and 5], which is translated between a UHV chamber mounted on top of the cryostat and a cryogenic insert [Fig. 4]. Samples and tips are exchanged at room temperature when the STM module is in the top UHV chamber and then the whole module is lowered into the insert using a long linear translator. The cryogenic insert consists of a UHV vacuum tube, which contains a copper cone spliced in the stainless steel tube in the bottom section, together with a custom receptacle wired to a multi-pin ceramic feedthrough on the bottom. The STM module [Fig. 4] uses 18 shear piezoelectric motors for coarse xyz positioning, a 12.7 mm OD piezoelectric tube for xy scanning, and a separate 19.05 mm OD piezoelectric tube for fine z motion. The STM module shell is constructed out of molybdenum [Fig. 5], which has low thermal expansion combined with good thermal conductivity. The photo in Fig. 5 shows the STM module with a spring loaded locking stage on top of it with guiding Teflon rollers.

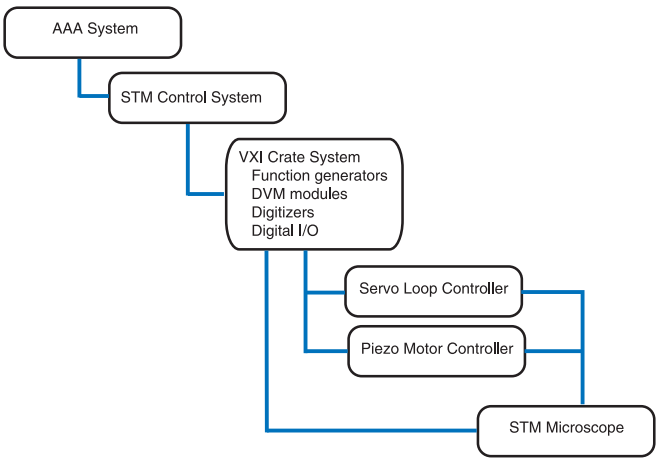

FIG. 2. Block diagram of AAA and STM control systems.

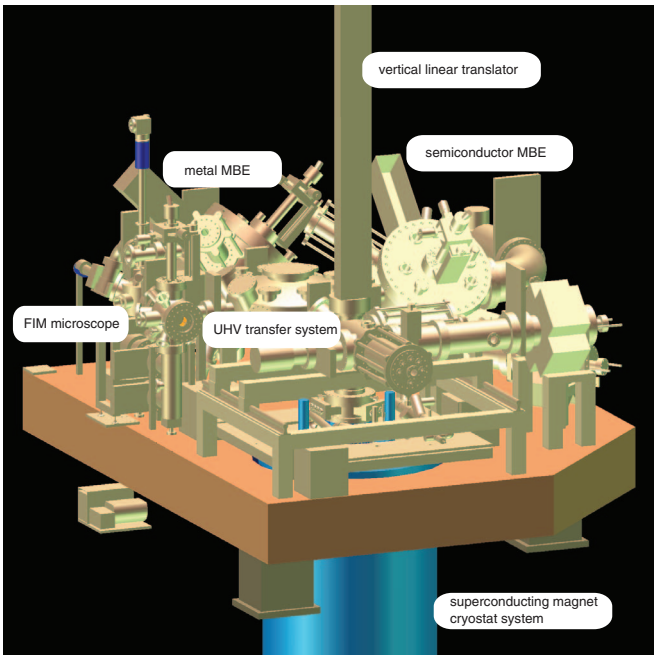

FIG. 3. CAD image of the cryogenic STM/AAA system.

The upper STM chamber contains a horizontally mounted translator incorporating three evaporators for metal deposition. With the STM module in the cryostat, different atoms to be used in the atom manipulation process can be evaporated onto a cooled substrate by positioning the appropriate evaporator over the UHV tube going into the cryostat. Typical deposition rates, as measured with a quartz crystal monitor about 2 cm below the evaporator in the upper chamber, were 3.3 nm/min resulting in a deposition rate on the sample of 0.08 pm/min. Typical deposition times were 1 min yielding 3.3 nm on the monitor, and ≈0.001 nm on the surface due to the long distance between the sample in the cryostat and evaporators in the upper chamber. For gas molecules like CO, we filled the upper chamber to 1.33×10^{-4} Pa for 25 s, resulting in a surface coverage of ≈0.03 ML.

All examples of autonomous atom assembly shown in this article use the lateral manipulation of Co atoms or CO molecules that have been deposited onto a Cu(111) crystal. The Cu crystal was cleaned by repeated cycles of Ne ion sputtering and annealing to approximately 600 °C. The Cu(111) surface, shown schematically in Fig. 6, contains two distinct 3-fold hollow sites, which are hcp or fcc stacked depending on if there is an atom below the hollow or not in the 2nd

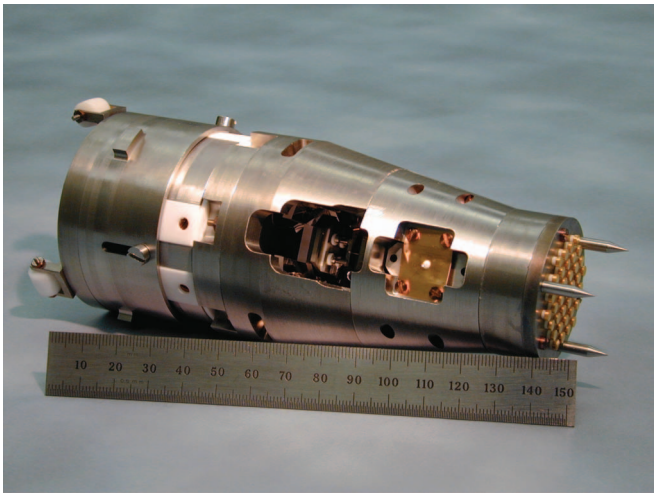

FIG. 5. Picture of the STM module with the locking compression stage on top and electrical contacts on the bottom. The module shell is made out of molybdenum.

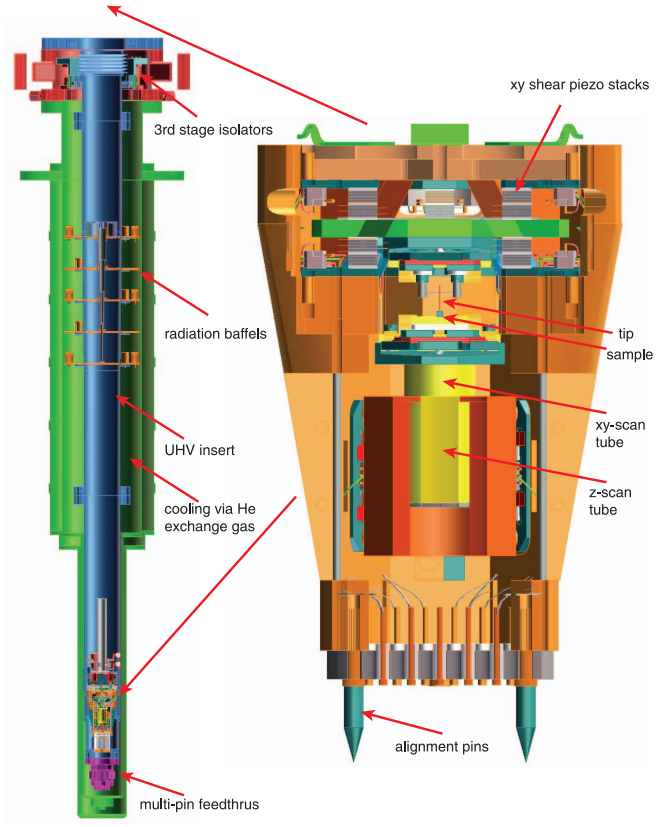

FIG. 4. CAD images of the UHV cryogenic insert (left) and the STM module (right). The STM module is translated from the vacuum chamber on the top of the insert (not shown) to the bottom of the insert where it makes contact to a wired plug receptacle. The cables connect from the multi-pin through the exchange gas region to the top of the insert.

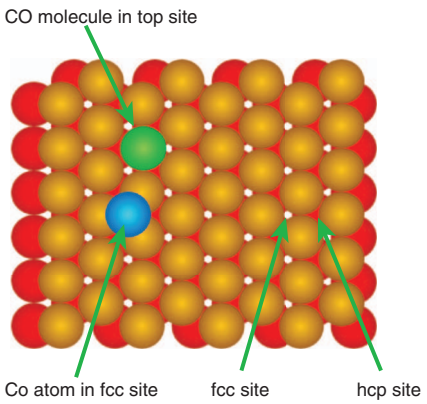

FIG. 6. Schematic top view of the Cu(111) surface showing the top two layers. The fcc and hcp sites are indicated with the hcp site above an atom in the 2nd layer. A Co atom is shown in its natural fcc binding site but can be manipulated to the hcp site using atom manipulation with the STM probe tip. A CO molecule is shown in its on top binding site.

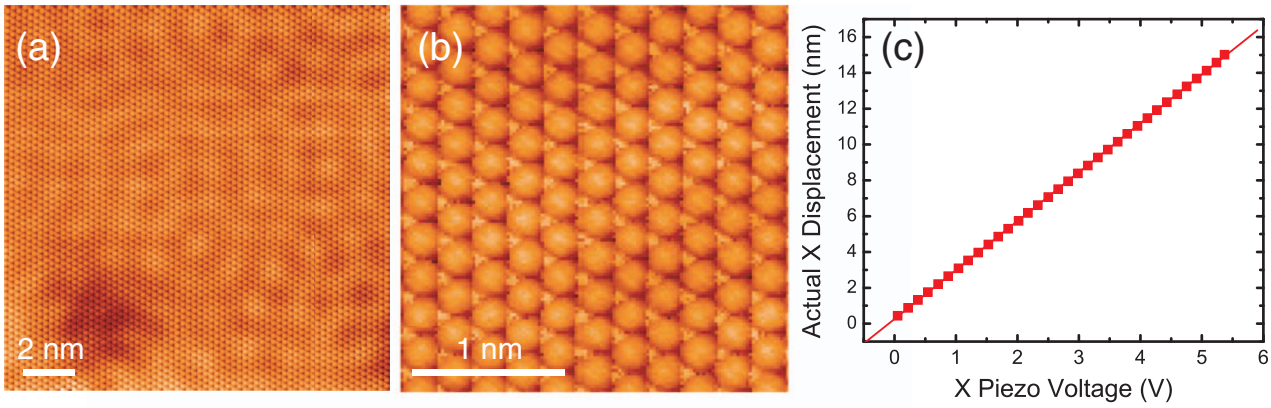

FIG. 7. (a) Atom manipulation image made from manipulating a Co atom on a Cu(111) surface. Image size 15 nm × 15 nm, tunneling current 50 nA, sample bias −5 mV. (b) Zoomed in image of (a). The color scale covers a height range of 44 pm for (a) and (b). (c) X displacement measured from lattice positions in (a) versus applied X piezo voltage.

Cu layer. Co adatoms prefer to bind in the fcc site, but can be forced into the hcp site using the tip interaction during atom manipulation [see Fig. 7].[23] CO atoms bind preferentially to the on-top sites of the Cu(111) surface. Iridium probe tips were used for this work; they were cleaned via heating and field evaporation in a field ion microscope [Fig. 3]. Final tip conditioning was achieved by controlled poking of the tip into the substrate and then checked using atom manipulation imaging as described below [Fig. 7]. All measurements and manipulation were made with the sample at a temperature of 4.3 K.

III. PLANNING AND EXECUTION METHOD

The first task required to autonomously build a nanostructure one-atom-at-a-time from a random array of adsorbed atoms involves deciding the sequence of atoms to move and the paths they will move along. This process is called path planning. It is the art of deciding which route to take based on, and expressed in terms of, the current internal representation of the terrain, which in our case is an atomic lattice. Path planning is used in many robotic applications ranging from automatic driving or piloting of vehicles or aircraft to obtaining driving directions from web based or in-car mapping systems. The specific protocol in our AAA implementation to build nanostructures follows similar path planning concepts and includes the following steps:

(1) A precise calibration of the piezo actuators used to raster scan the probe tip for STM imaging is performed to assure accurate positioning and measurement.
(2) The geometry, dimensions, and orientation of the substrate lattice are measured.
(3) The AAA system identifies adatoms and obstacles from the STM image using pattern recognition, and locates these positions relative to the substrate lattice.
(4) A design for the desired structure is specified and communicated to the AAA system by providing the lattice coordinates of the final configuration of atoms.
(5) A path planning algorithm is applied to analyze the initial and desired final atom configurations and determine all the atom move paths necessary to build the required nanostructure. Extra atoms are stored in "parking lots" surrounding the nanostructure.
(6) The AAA system executes the computed sequence of adatom moves by directing the STM control system to build the desired nanostructure. A virtual display of the tip motion over the substrate is simultaneously displayed by the AAA computer system. System options include imaging a portion of the construction area after each atom move to examine in detail the assembly process; this allows, for example, verification that the actual constructed geometry is identical to the virtual display of the plan.

We discuss specific aspects of each of the steps in more detail below.

A. Substrate lattice

The precise placement of atoms to an exact lattice location in atom manipulation requires being able to accurately and reproducibly move the actuating tip to any given lattice location. As a first step, a highly accurate calibration of the piezo actuators used in the STM must be performed. This requirement is particularly stringent in the case of the AAA system which, absent a closed positioning control loop, requires the placement of adatoms on the substrate crystal lattice with a precision significantly better than one lattice constant.

We have calibrated our piezo actuators by rastering an adatom over the surface using atom manipulation to create an atom manipulation image [Figs. 7(a) and 7(b)].[23] An atom manipulation image displays the physical structure of the underlying substrate lattice with an enhanced corrugation even when the lattice is not visible in a regular STM topograph, as is typically the case on close-packed metal surfaces where the charge density corrugations are a few pm. The two main features in the Co atom manipulation image of Fig. 7(b), namely, the larger round spheres and the fuzzy triangles between them,

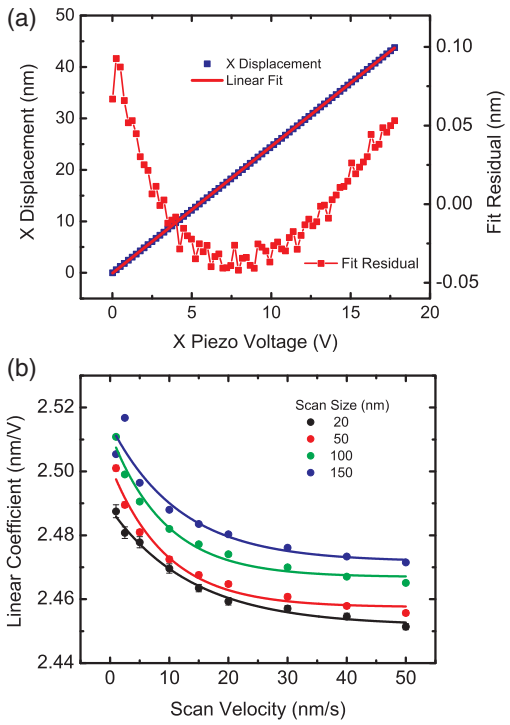

FIG. 8. Nonlinear behavior in piezoelectric scanner. (a) Measured X displacement from the lattice positions on an InAs(110) cleaved surface vs applied X piezo voltage. Scan velocity 20 nn/s. Deviations from a linear fit are shown on the right axis. (b) Linear calibration coefficients obtained from scanning an InAs(110) cleaved surface as in (a) vs scan velocity for various scan sizes. The solid lines are a fit to a single exponential decay.

represent the fcc and hcp binding sites of the Co atom in the Cu(111) lattice, respectively. The hcp sites displays a smaller feature because it is a metastable binding site and the Co only binds there with the tip forcing it into this location.[23] The measurement and analysis of an atom manipulation image allows the calibration of the piezo actuators to better than 1% [Fig. 7(c)]. Unfortunately, piezo actuators are nonlinear devices which are prone to hysteresis and creep. In practice, this limits the distance over which the calibration procedure is useful. For larger distance calibration and its speed dependence, a cleaved InAs(110) crystal surface is very useful as the terraces can be atomically flat on the micrometer scale. Figure 8(a) shows a calibration using the InAs(110) lattice over a 45 nm distance. The residuals from the linear fit show deviations approaching 0.1 nm on this length scale at the ends of the scan range. Additionally, hysteresis and creep cause the calibration to be dependent on scan velocity, which is typically different for the case of moving the adatoms versus topographic imaging. Figure 8(b) shows the calibration dependence on scan velocity for different image sizes. A typical atom move velocity may be 1 nm/s, whereas imaging may use 30 nm/s. One observes from Figure 8(b) that the calibration can vary ≈1% or 2% between these values. A one lattice site error (0.255 nm) in placement is thus likely to occur when the error in calibration reaches about $\frac{1}{2}$ of one lattice constant, or ≈0.1 nm. From Figs. 8(a) and 8(b), this occurs with larger scan sizes approaching 100 nm or more significantly when different velocities and scan sizes are used for moving atoms and imaging. These considerations lead to practical

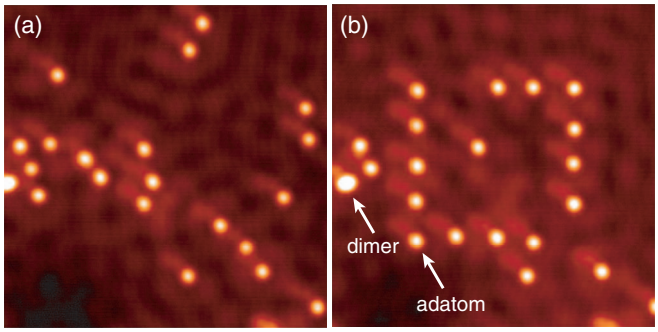

FIG. 9. STM images of single Co adatoms and a dimer (two bonded Co atoms) on the Cu(111) surface. Obstacles like the dimer are avoided in the atom assembly. (a) Initial random configuration of Co atoms. (b) STM image after partial assembly of a square pattern. Image size, 15 nm × 15 nm, tunneling current 1 nA, sample bias −10 mV. The color scale covers a height range of 105 pm for (a) and (b).

limitations on the range over which the assembly process can take place without implementing further corrections for nonlinear actuation and creep in the piezo actuators, as discussed in depth in Sec. IV. We have overcome this limitation by implementing a multi-pass path planning algorithm that builds large structures piecewise, as will be discussed below. Following the atom manipulation imaging and piezo actuator calibration, the crystalline substrate geometry, dimensions, and orientation are known to the AAA control computer.

B. Identifying adatoms and obstacles

In the current embodiment of AAA, the initial configuration of adatoms to be manipulated is created via physical vapor deposition of Co atoms onto a cold Cu(111) substrate. This produces a random pattern of adatoms since surface diffusion is inhibited at these temperatures [Fig. 9(a)]. The AAA controller initiates the assembly process by directing the STM system to image the adsorbate covered substrate surface. The area to be imaged is set to a size slightly larger than required for the desired nanostructure. After obtaining the image, the AAA system determines the location of each adatom by analyzing the topographic image. The computer algorithms used to identify and spatially locate adatoms are based on topographic height thresholding and an estimation of the adatom area expected in the image; these parameters are user defined and set in advance through the AAA control system graphical user interface. Similarly, obstacles are identified when analysis of the topograph reveals height thresholds and adatom areas exceeding the boundaries defined as characteristic of a single adatom. Typical anomalies identified as obstacles are adatom dimers, substrate vacancies, or impurities [Fig. 9(b)]. Such obstacles usually cannot be manipulated and are, therefore, to be avoided during atom assembly.

C. Nanostructure input

The desired nanostructure geometry is first defined by the user through a simple drawing program that specifies the desired relative positions of all adatoms and produces a list of the (x, y) coordinates of each adatom relative to an origin that is typically coincident with one of the adatoms. Having

access to the list of desired relative (x, y) positions that define the nanostructure geometry, the AAA control program then aligns the relative geometry of the desired nanostructure with the available substrate sites that have been determined in the already calibrated laboratory coordinate system and displays an overlay of the nanostructure geometry on the surface in the computer display. The user has the flexibility to use the graphical user interface to overlay the pattern anywhere within the scanned area that was defined in Sec. III B above. Since the AAA control computer will not attempt to move obstacles, e.g., dimers and other non-single adatom objects, it is advantageous to locate the pattern in an area free of obstacles.

D. Path planning the autonomous assembly

Path planning lies at the heart of the autonomous atom assembly process. The goal of the path planner is to construct the pattern described in Sec. III C along with an adatom-free zone surrounding the pattern. The area consisting of the pattern zone and adatom-free zones is known as the building zone.

1. Sizing and locating the building zone

Once the user has determined the construction location, the AAA executes an automatic procedure that ensures that the number of adatoms in the building zone equals the number of adatoms that are required to construct the pattern. If not enough adatoms are available, the building zone is symmetrically expanded about its center until enough adatoms are located. If too many adatoms exist in the building zone, a "parking zone" is established outside of the current building zone where the extra atoms may be placed in an easily constructible pattern. These parking locations are then added as construction goals, and the building zone is automatically expanded to include the pattern, the adatom-free zone, and the parking zone.

2. Pattern decomposition

Due to the limitations on the atom placement precision in the AAA system discussed in Sec. III A, precise one-pass construction of large patterns can be difficult and may contain errors in atom placement. These errors would be the difference in the adatom position after manipulation from its specified goal position, and would be in multiples of the crystal lattice spacing. Therefore, we have chosen to decompose large patterns into smaller areas, i.e., planning regions that can be constructed perfectly. Figure 10 shows one such decomposition for a square pattern. The key requirement is that each new planning region must have at least one adatom in common with an already finished area of the pattern; this shared adatom is known as the anchor. The use of anchor atoms along with the precisely regular underlying crystallographic structure is sufficient to completely eliminate all inaccuracies due to the nonlinearity and drift of the piezo actuator system in the AAA.

The purpose of the pattern decomposition process is to determine a near optimal sequence of regions to be built by the

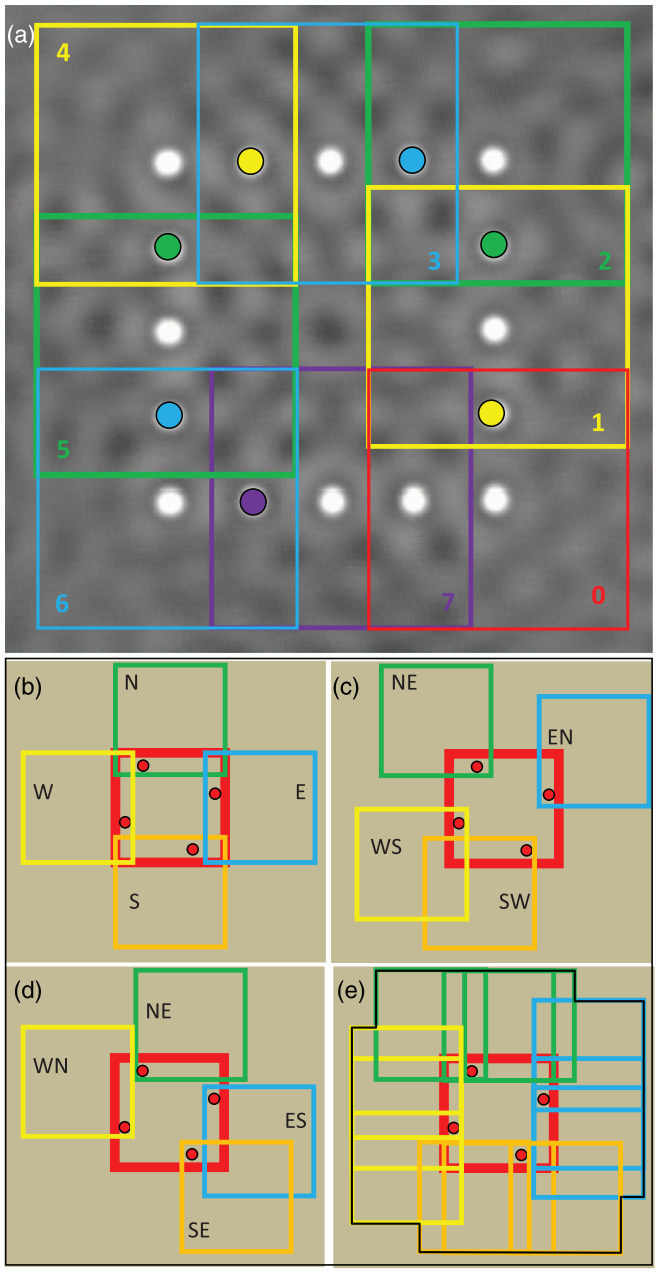

FIG. 10. (a) Example of pattern decomposition into registered planning regions. The decomposition begins with the red square that contains the lower right adatom site and proceeds through the use of a depth-first search. The decomposition order may be seen by following the regions that match the number sequence. The decomposition is complete when the purple region is achieved (region 7). The circular color overlay shows the "anchor" adatom that is used for registration between regions. (b)–(e) Possible placement of regions to build off of central red region. The extreme north, south, east, and west adatoms are identified and three possible new regions are examined that will utilize these extreme adatoms as anchors. Figures (b)–(d) depict these configuration, while figure (e) depicts the combined space. The first letter in each box represents the location of the extreme adatoms. The second letter represents the placement of the region with respect to this adatom.

AAA system. This sequence is determined by a planning technique known as graph search, which overlays a directed graph of possible planning region locations over the entire pattern. A directed graph is a set of nodes, connected by edges, each of which has an associated direction. As shown in Fig 10(a), the first planning region selected contains the lower-right area of the pattern. A depth-first search is then performed to

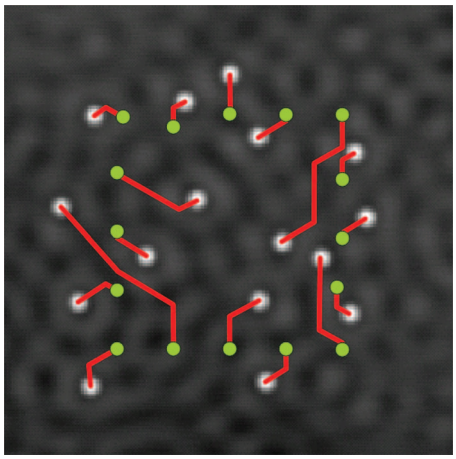

FIG. 11. Rough-pass adatom moves for the construction of a simple square pattern. The underlying image is of a Cu(111) surface with Co adatoms that will be used in the construction. The red-lines represent the planned paths for the adatoms and the green dots are their final resting places for the rough pass plan. The paths are planned for sequential moves in a manner that will preclude adatoms from coming too close to other adatoms or obstacles.

determine a combination of planning regions that will provide coverage of the entire pattern.[39] A depth-first search explores each alternative path to its logical end before trying a new path.

To apply this search to determine an ordered set of planning regions, we dynamically construct a planning graph by assuming that each planning region may be connected to 12 adjacent "child" regions. A child region is defined as a planning region that is offset from the current region in a given direction such that is shares the smallest number of adatoms (but at least one) with the parent region [Fig. 10]. As the search proceeds, each child planning region is examined to see if it encompasses any adatoms that have not been assigned to an existing planning region. If it does, the encompassed adatoms are assigned to this child region and the search proceeds from there by this child producing 12 new children. If the current child region does not contain any unassigned adatoms, then it is deleted and the search proceeds to the next of this region's 11 siblings. If all 12 siblings have been considered with no new adatoms being added, the search will backtrack to the parent of the current region, and one of the parent region's siblings will be considered. The search proceeds until all of the destination lattice sites have been included in the plan. Due to the nature of depth-first searches and the constraints placed on the size of the building zone, the search is guaranteed to find a solution if it exists, but the solution is not guaranteed to be optimal. The only condition that will cause a pattern to fail to be decomposed is if the desired final pattern contains atoms spaced so far apart that every atom and its nearest neighbor cannot fit within a planning region.

3. Rough-pass planning

Once we have selected our ordered set of planning regions, it is possible to determine the number of adatoms that will be needed in each planning region. The goal of the rough-pass planning system is to assure that the correct number of

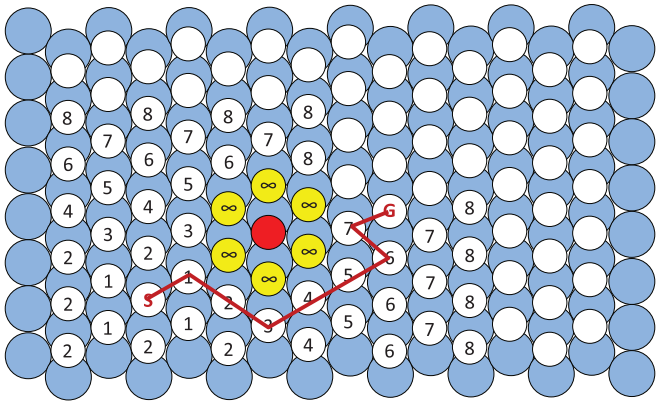

FIG. 12. Graphical example of uniform cost search. In this figure, the red object represents an obstacle and the yellow ring around the obstacle is a "keep-out" zone. Nodes in the graph (white circles) are located at every potential adatom site and the nodes are connected to all possible neighbors. The location marked with a "S" is the adatom starting location and the location marked with a "G" is the goal location. The blue spheres depict the material substrate. The cost of moving between two adjacent circles is "1 unit", while the cost of entering the obstacle keep-out zone is infinity. A uniform cost search expands the cheapest unexpanded node. This causes a radial search pattern from the origin when no obstacles are encountered. The number on the circle shows the cost reaching that site. This search will reach the goal with a final cost of 8 and will contain an unnecessary turn. The adatom locations are shown in bridge sites for illustration and the actual binding site will depend on the type of adatom or molecule.

adatoms is located in each planning region while minimizing the number of moves that the AAA will need to perform. This is accomplished by assigning each adatom to a specific final, or goal, location. Each adatom is assigned to its nearest unassigned goal location. If two adatoms share the same nearest goal location, then the closer of the two will receive the assignment and the other adatom will attempt its next nearest goal location. Any adatom that does not reside in the same planning region as its assigned goal is scheduled to be moved by the AAA system. The adatom will be moved into

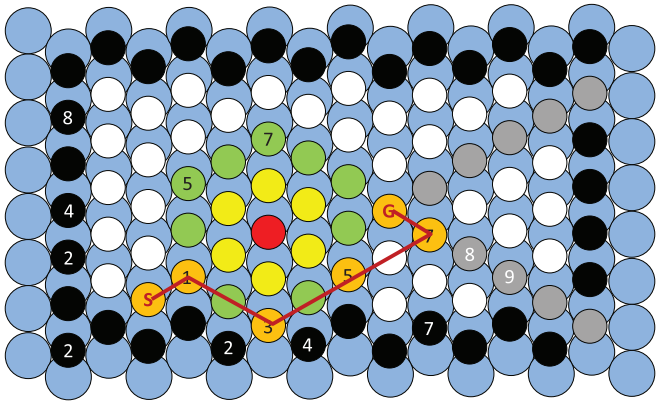

FIG. 13. Graphical example of incrementally created graph structure. For this graph, nodes only exist in environmentally relevant locations. As shown, nodes are placed in fields surrounding obstacles (light green circles), as boundaries on the edge of the building zone (black circles), and as "runways" leading to the goal (grey circles). The cost of traversing an edge is based on its feature type; the cost is uniform far from an obstacle and increases as the obstacle is approached. As may be seen, this technique tends to avoid unnecessary turns and produce straight paths that directly proceed to the goal. The adatom locations are shown in bridge sites for illustration and the actual binding site will depend on the type of adatom or molecule.

the proper region and placed in a location that is deemed to be "safe," meaning that it will not be perturbed by its proximity to an obstacle or the future planned trajectory of another adatom.

An example of one such rough plan is shown in Fig. 11. As may be seen from this figure, the general shape is formed for the final construction. However, constraints that are designed to provide for collision free placement and movement of adatoms during longer moves preclude several adatoms being placed in their true final locations. The actual path that will be followed is determined by the path planner as described below and shown as a red path in Fig. 11.

4. Fine-tune planning

As a result of the rough-pass planning, each planning region should now contain the correct number of adatoms for construction. The precise pattern can now be constructed. Since the order of the region's construction is based on the results of the original depth-first search, all but the first region will contain a precisely located anchor. By using this anchor as a fiducial mark, each region's pattern locations are assured to be globally correct.

The same technique utilized during the rough-pass planning is also utilized during the fine-tune planning to match adatoms to goal locations. The adatoms are moved to their precise goal locations following their prescribed path as determined by the technique described below. For construction of small patterns, it is possible that only the fine-tuning pass of the system is necessary. For early constructions, this was the case and only one planning region was utilized. This is discussed further in Sec. IV. On the other hand, it is possible that unanticipated placement errors could occur, even in a small planning region. For this reason, an option is provided in the AAA to specify that the planning region should be reimaged following assembly to verify an accurate construction. If an error exists, new plans are then created to automatically correct the misplaced adatoms.

5. Path planning

The path planning portion of the system computes safe trajectories that adatoms should travel from their initial positions to their selected goal locations. We have constrained the paths to allow moves only along the substrate crystallographic directions. This constraint is imposed since the

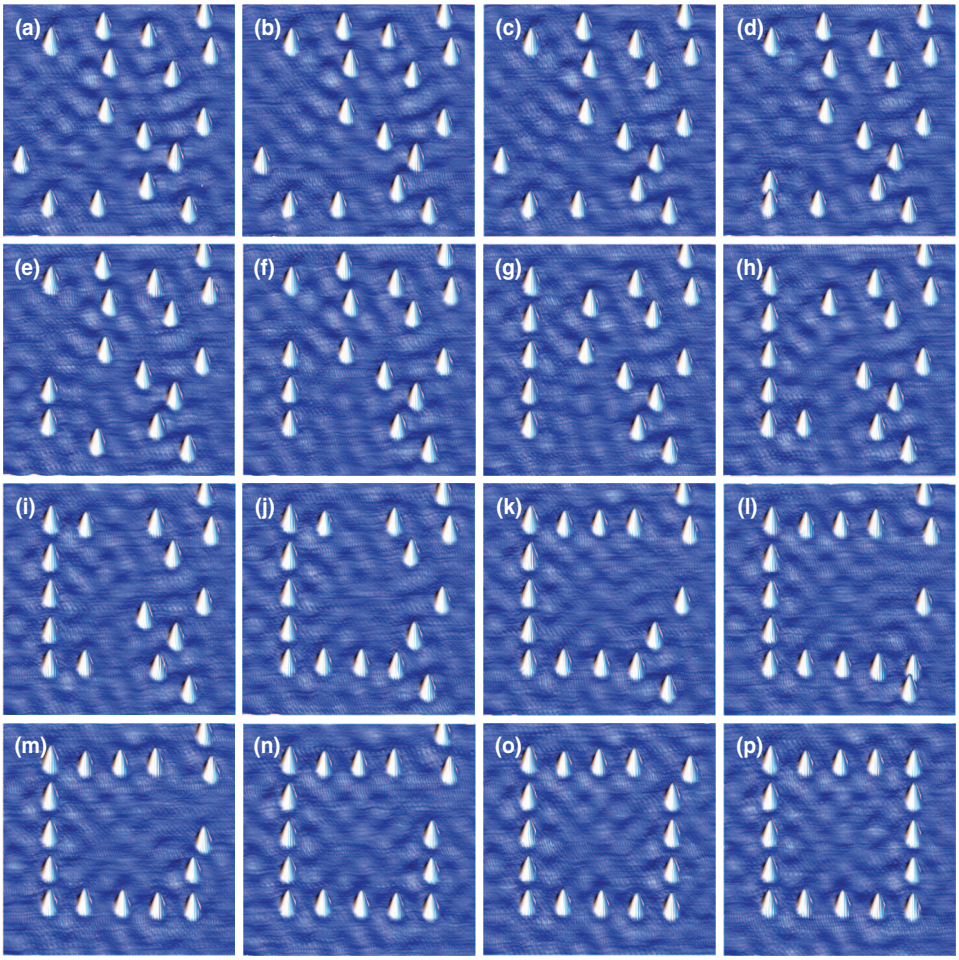

FIG. 14. Autonomous assembly of a simple square from a random arrangement of Co atom on Cu(111) using a single pass plan. (a) Initial random arrangement of Co atoms. (b)–(p) Sequence of images after each atom move. Image size 15 nm × 15 nm. Tunneling current for imaging, 1 nA, sample bias −10 mV, image impedance 10 MΩ. Tunneling current for manipulation, 100 nA, sample bias −10 mV, manipulation impedance 100 kΩ. T = 4.3 K. Images are shown in colored 3D top view with light shadowing with a height range of ≈100 pm.

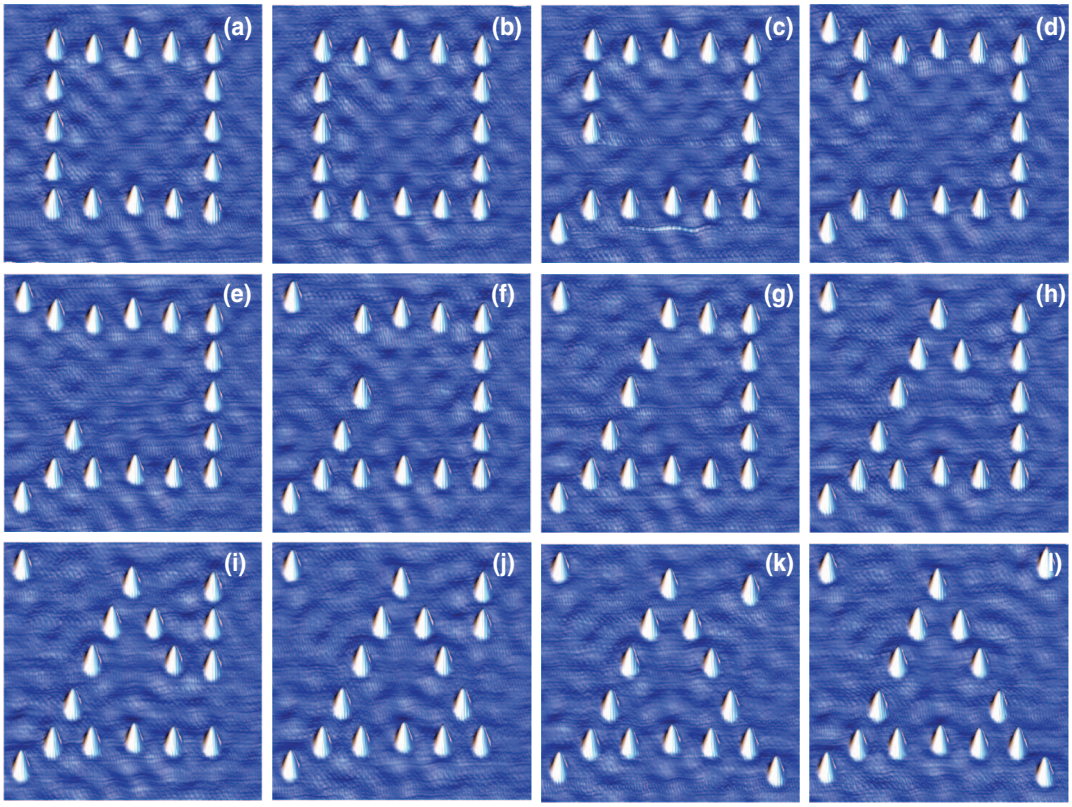

FIG. 15. Autonomous assembly of a simple triangle on Cu(111) using a single pass plan starting from a simple square pattern of Co atoms from the assembly show in Fig. 14. (a) Initial arrangement of Co atoms. (b)–(l) Sequence of images after each atom move. Image size 15 nm × 15 nm. Tunneling current for imaging, 1 nA, sample bias −10 mV, image impedance 10 MΩ. Tunneling current for manipulation, 100 nA, sample bias −10 mV, manipulation impedance 100 kΩ. T = 4.3 K. Images are shown in colored 3D top view with light shadowing with a height range of ≈100 pm.

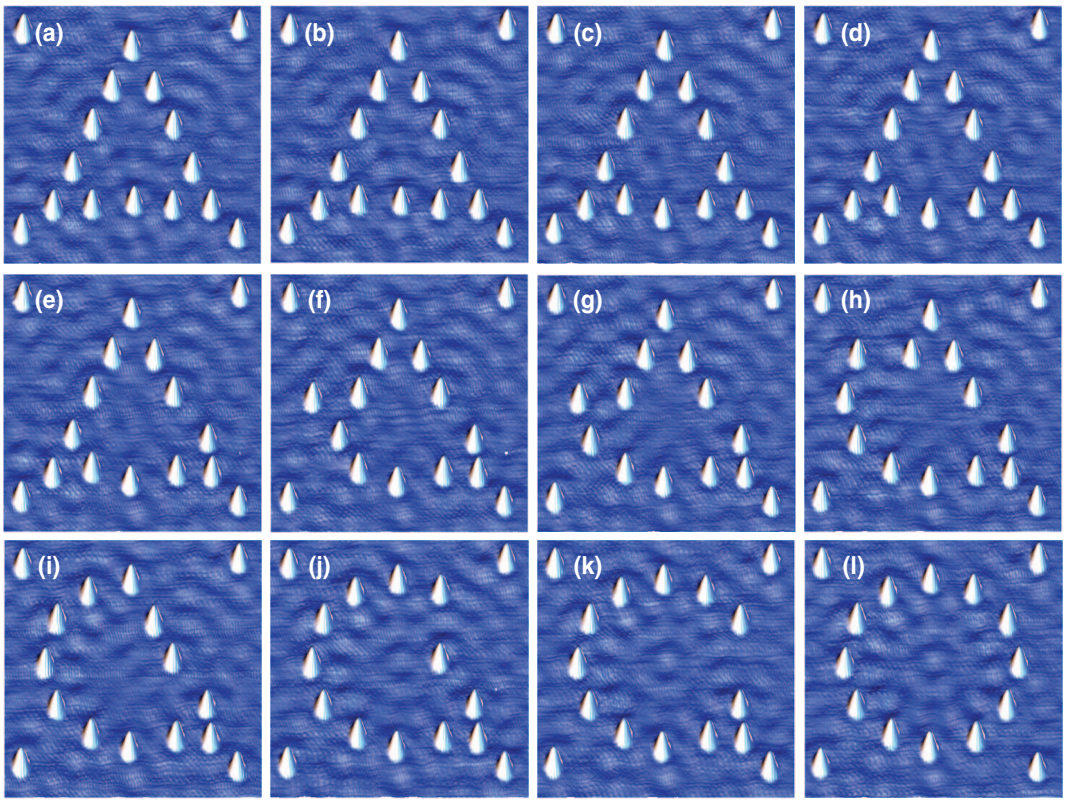

FIG. 16. Autonomous assembly of a simple circle on Cu(111) using a single pass plan starting from a simple triangle pattern of Co atoms from the assembly shown in Fig. 15. (a) Initial arrangement of Co atoms. (b)–(l) Sequence of images after each atom move. Image size 15 nm × 15 nm. Tunneling current for imaging, 1 nA, sample bias −10 mV, image impedance 10 MΩ. Tunneling current for manipulation, 100 nA, sample bias −10 mV, manipulation impedance 100 kΩ. T = 4.3 K. Images are shown in colored 3D top view with light shadowing with a height range of ≈100 pm.

barriers to movement are typically lower along certain crystal directions, i.e., along the troughs in the crystal lattice. An additionally imposed constraint is that adatoms cannot be moved into obstacle regions, i.e., within a preset distance of an obstacle or adatom. Path construction is performed by utilizing a traditional uniform cost search approach [Fig. 12], also known as a Dijkstra search.[40] Uniform cost searches require an underlying graph that is searched to find a solution. The simplest mapping of the lattice to a graph structure is to allow each possible adatom lattice position to be a node in the graph, and to connect each node with a graph edge, i.e., path segment, to its nearest neighbors along crystallographic directions. Path segments that connect to an obstacle region are given infinite cost, thus eliminating them during the search. However, this graph structure was found to produce paths with a large number of unnecessary turns. It was found that paths with fewer turns were found by utilizing an incrementally created graph structure [Fig. 9].[41]

For incrementally created graphs, graph nodes are created and connected during the search process in relevant locations. The definition of relevant locations varies from application to application. In our case as shown in Fig. 13, relevant locations include lattice positions that are near obstacles, lattice positions along the boundary of the building zone, and "runways" leading to the adatoms desired goal. Here a runway is defined as a straight approach along a crystallographic direction to the goal. The cost of the graph's edge connections is based on the edge's length and its proximity to an obstacle. This allows for the creation of a "repulsive field" that pushes the path away from obstacles.

A standard Dijkstra search is still utilized. The main difference is that as a node is evaluated, the nearest relevant location along the crystallographic directions of travel is connected with an edge. A Dijkstra search is complete and optimal. This means that the best combination of relevant locations will be found as the adatom's final path.

E. Assembly execution

Once all the atom move paths are determined, the AAA system issues orders to the STM control system to sequentially move each atom. In turn, each atom move incorporates the following sequence: The tip is moved to the initial atom location with the tip voltage set at a value that provides the tunneling impedance used for topographic imaging, i.e., the "topographic image impedance." The tunneling impedance is then lowered to the "atom-move impedance." This causes the tip to move closer to the adatom and forms a temporary bond with the adatom. The tip is then moved along the predetermined path at a specified move speed with the tunneling impedance remaining at the atom-move value. When the tip reaches the end point of the predetermined path, i.e., the final atom position, the tunneling impedance is turned back to the topographic image value and, consequently, the tip withdraws and releases the adatom at the goal position. The AAA control system then either takes a verification image of the area, if this option has been selected, or goes on to the location of the next atom to be moved.

IV. RESULTS

In this section, we describe our initial results using the AAA system to construct a variety of simple geometric nanostructures demonstrating quantum confinement and engineered "molecular" bonding and anti-bonding states. We first describe the construction of simple geometric shapes using a single pass AAA construction. We show that this results in small adatom placement errors, which can be removed by running the AAA system iteratively to improve the final outcome. In Sec. IV B, we show the improvement in construction of the nanostructures using the multiple region construction algorithm, where perfect confining nanostructures are built. Finally, in Sec. IV C, we demonstrate the use of the AAA as a scientific quantum toolkit to construct artificial lattice structures with CO molecules, where interacting quantum dots are

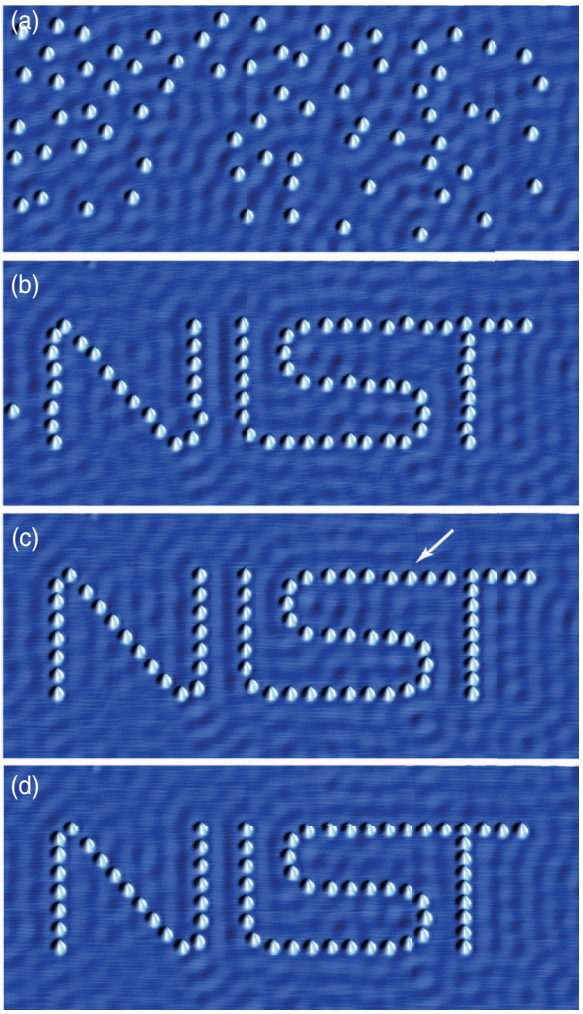

FIG. 17. Autonomous assembly of the NIST logo. (a) Initial random pattern of 71 Co atoms (a). (b) After 1st autonomous construction starting from the random pattern in (a). Total construction time 31 min. (c) 2nd autonomous construction starting from pattern in (b). A few atoms still out of place at end of "S" near arrow. Total construction time 12 min. (d) Perfect assembly of NIST logo after 4th autonomous assembly. Image sizes 40 nm × 17 nm. Tunneling current for imaging, 1 nA, sample bias −10 mV, image impedance 10 MΩ. Tunneling current for manipulation, 100 nA, sample bias −8 mV, manipulation impedance 80 kΩ. T = 4.3 K. Images are shown in colored 3D top view with light shadowing.

created by the removal of CO molecules from the artificial lattice.

A. Single region construction of a square, triangle, and circle nanostructure

The performance of the autonomous atom assembler is illustrated by the sequential construction of three simple shapes: a square, a triangle, and a circle, starting from a random arrangement of 16 cobalt atoms that have been deposited within of a 15 nm × 15 nm area. Figure 14(a) shows the initial configuration of adatoms in a STM topographic image. After this image is recorded, the sequence of events to build a structure autonomously is as follows. The AAA control system analyses the topographic image of this area, identifies the adatoms and their locations, and displays a virtual world view of the area. The AAA system then waits for the user to input a desired structure by selecting from a collection of files, each of which defines the geometry of a different nanostructure. In this case, we selected a square composed of 16 adatoms. The AAA control computer, knowing both the position of each randomly situated adatom to be used as

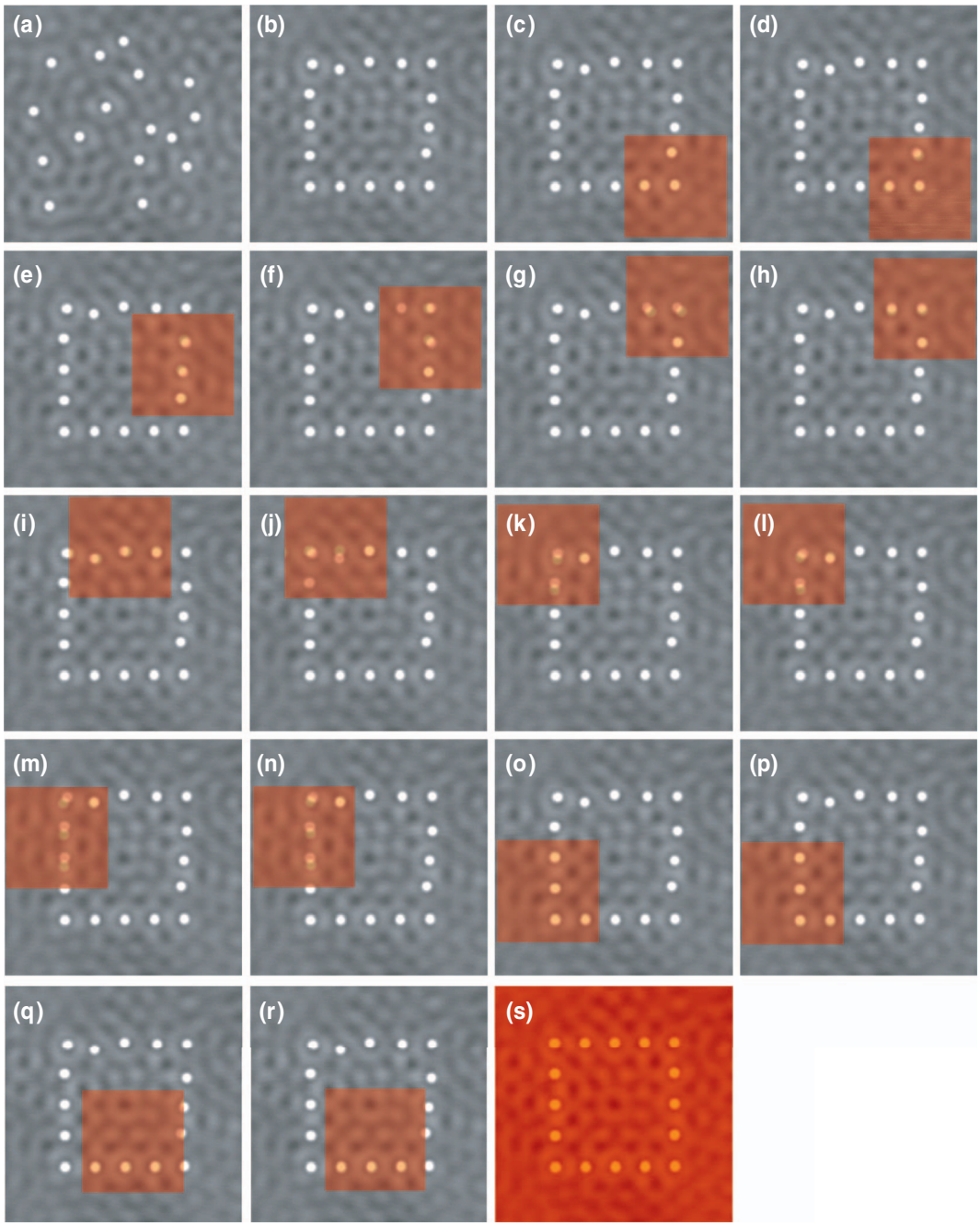

FIG. 18. Autonomous assembly of a simple square of Co atoms on Cu(111) using a multi-region planner. (a) Initial random pattern. (b) Result after rough single pass of the planner. (c)–(r) Small region assemblies shown in color overlaid onto the rough pass results. (s) Final construction of a perfect square pattern. Image size 17.5 nm × 17.5 nm. Tunneling current for imaging, 1 nA, sample bias −10 mV, image impedance 10 MΩ. Tunneling current for manipulation, 100 nA, sample bias −10 mV, manipulation impedance 100 kΩ. T = 4.3 K. The grey color scale covers a height range of 100 pm for (a)–(r).

building material and the specific geometry and position of the desired nanostructure, then proceeds to calculate a complete plan incorporating a series of atom moves along specific paths. The user then selects the build button, which starts the AAA system building the structure by sending commands to the STM control system to first move the tip over an atom in the plan, acquire the atom by turning on the tip-adatom force (lowering the junction impedance), moving the adatom to a new location, and then finally releasing the adatom (raising the junction impedance). In Fig. 14, we show a few snapshots, i.e., topographic images, of the various atom configurations taken during an autonomous construction of a square. During the autonomous assembly process, the tip motion and atom moves are shown in a virtual display (see the supplementary material[45] for the full sequence of assembly). As the pattern progresses, we can see changes in the background, which are due to scattering interference patterns in the two-dimensional electron system at the Cu(111) surface. As each atom is moved to a new location, the location of the scattering centers (the adatoms) changes and a new interference pattern is created. Quantized electronic states are created for confining geometries, which can be probed with the spectroscopic capabilities of the STM.[8,9]

Figure 15 shows a triangular confining geometry constructed with the previous square construction as the starting point, followed by the construction of circular confining geometry [Fig. 16] from the triangle structure. Since the triangle and circle use only 12 of the 16 atoms, the remaining four atoms are placed in the four corners. As imaged in the background modulations surrounding the atoms in their final configurations, the final states of the two-dimensional electron systems show highly symmetric electron density patterns reflecting the Fermi-level scattered interference patterns.

In examining the final structures, we observe that the square and triangle constructions are not perfect, i.e., as designed, in these single region plans. The errors generally arise from inaccuracies in the piezo calibration, particularly the dependence on scanning velocity which is different for manipulating atoms versus topographic imaging. For larger patterns, these errors will increase as the nonlinear errors in piezo positioning increase. Such errors can frequently be dealt with by running the AAA system again taking the nearly perfect arrangement as the starting point. An example of a larger single pass construction is shown in the fabrication of the "NIST" logo [Fig. 17] with 70 atoms over a 40 nm × 17 nm area where we see multiple placement errors occurring [Fig. 17(b)]. The majority of placement errors are one lattice constant from the ideal positions. This particular example in Fig. 17(b) had more placement errors than usual possibly due to a non-optimal probe tip geometry. However, the errors were removed by simply running the AAA system again taking Fig. 17(b) as input with the outcome shown in Fig. 17(c). The errors were reduced from approximately 18 atoms out of place in Fig. 17(b) to 3 in Fig. 17(c) [see arrow at end of "S"], again with the errors being one lattice constant from the ideal positions. A perfect logo was converged upon after the fourth iteration, as shown in Fig. 17(d). The time for construction of the logo in Fig. 17(b) was about 31 min. The majority of this time is due to the tip velocity used to move the atoms, which was a conservative 1 nm/s to avoid dropping an atom during travel. The construction time could be decreased proportionally by increasing the atom move velocity. This was not investigated in detail, but factors of 2–10 increase in velocity should easily be possible. A faster velocity may require an increase in the "tip-adatom" force requiring lower manipulation impedances.

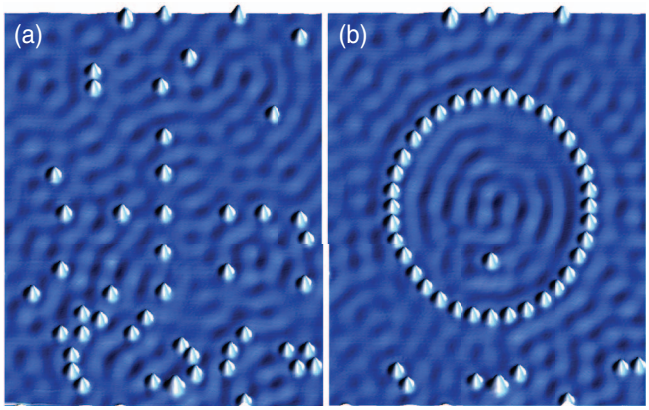

FIG. 19. Autonomous assembly of 38 Co atoms into an elliptical quantum coral with one atom at the bottom focus point with using a multi-region planner. (a) Initial random arrangement of Co atoms in a 20 nm × 25 nm region. (b) Final image after construction. Construction involved 40 multi-region passes each 3 nm × 3 nm. Total construction time 66 min. Tunneling current for imaging, 1 nA, sample bias 10 mV, image impedance 10 MΩ. Tunneling current for manipulation, 100 nA, sample bias 10 mV, manipulation impedance 100 kΩ. T = 4.3 K. Images are shown in colored 3D top view with light shadowing.

B. Multiple region construction of a square and elliptical nanostructure

To overcome the limitation of the piezo positioning errors we observed in Sec. IV A, we break the pattern into smaller "trusted" regions, where each of the trusted single plan regions is small enough to guarantee 100% accurate placement of atoms as described in Sec. III D above. Figure 18(a) shows a random arrangement of 16 Co atoms in a 17.5 nm × 17.5 nm assembly area. To construct the square pattern using the multi-region construction, the AAA first performs the pattern decomposition to determine the number and location of a series of small, trusted plan regions; the trusted plan region size is initially set by the user in the AAA build menu based on the parameters of the assembly, e.g., adatom, substrate, move speed, image speed, etc. To construct the square from the random arrangement of atoms in Fig. 18(a), the AAA decomposes the main region into 8 smaller, trusted regions of size 7.5 nm × 7.5 nm. The first, rough pass assembly endeavors to ensure the right number of atoms is present in the main (17.5 nm × 17.5 nm) assembly region and build the desired nanostructure, albeit with possible placement errors [Fig. 18(b)]. The construction then proceeds by building the structure piece-by-piece starting from the first small trusted region and proceeding to the next using one atom as an anchor that is shared between successive construction regions [Fig. 18]. The total construction sequence is best viewed in sequential frames as a movie file [see the supplementary

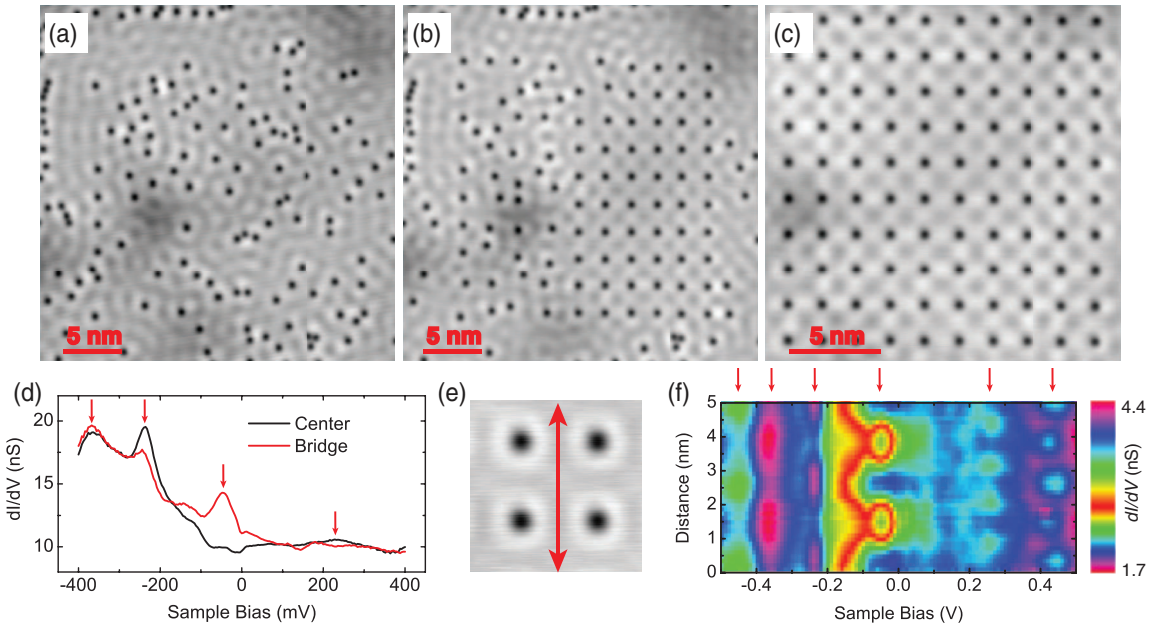

FIG. 20. Autonomous assembly of CO molecules into an ordered grid pattern with grid spacing 9a × 5√3a (2.3 nm × 2.2 nm) using a multi-pass planner. (a) STM topographic image of the initial random arrangement of CO molecules in a 30 nm × 30 nm region. (b) Image after partial construction. (c) Image of final construction assisted by some hand manipulation. (d) A comparison of tunneling spectra in the center of a 4-atom cell vs the bridge position showing quantum confined electronic states. (e) STM image of a 4-atom cell indicating the position of the tunneling spectroscopy shown in (f). (f) Differential tunneling conductance measured along the line in (e) showing quantum confined states with alternating nodal structure indicated by the red arrows at the top of the image. Tunneling current for imaging, 1 nA, sample bias 50 mV, image impedance 50 MΩ. Tunneling current for manipulation, 40 nA, sample bias 10 mV, manipulation impedance 250 kΩ. T = 4.3 K. The grey color scale covers a height range of 750 pm for (a)–(c) and 410 pm for (e).

material for the full sequence of assembly].[45] The final construction of the square pattern [Fig. 18(s)] using the multi-region construction is a perfect replica of the user specified square pattern.

Applying the multi-region construction to a more demanding challenge is shown in Fig. 19 in the construction of an elliptical quantum corral with a single atom at one of its foci using 38 atoms in a 20 nm × 25 nm region. Here the construction involved 40 multi-region passes, each 3 nm × 3 nm in size, resulting in a perfect elliptical construction. The total time of this autonomous construction was 66 min. Construction of this nanostructure by hand would take considerably longer, demonstrating the benefits of the AAA system. In this construction the time is split between moving the individual atoms, and the scan time for the multiple small regions. The construction time can be reduced if either of the atom move or imaging velocity is increased. We used very conservative velocities in this demonstration, and factors of 2–10 reduction in time should be possible.

C. Example: Construction of artificial atomic lattices and interacting quantum dots with CO molecules

The STM manipulation technique can additionally be applied to small molecules on surfaces.[10–12,15,25] One molecule that is frequently manipulated is the diatomic molecule CO. Early work showed that CO could be vertically switched reversibly between the surface and probe tip,[12] while newer work has shown that the CO molecule on the tip can be used as an atomic sensor.[42,43] Complex nanostructured geometries demonstrating logic functions have been created with CO molecules on Cu(111) surfaces.[19] Here we use the AAA assembler to laterally manipulate CO molecules on Cu(111) to

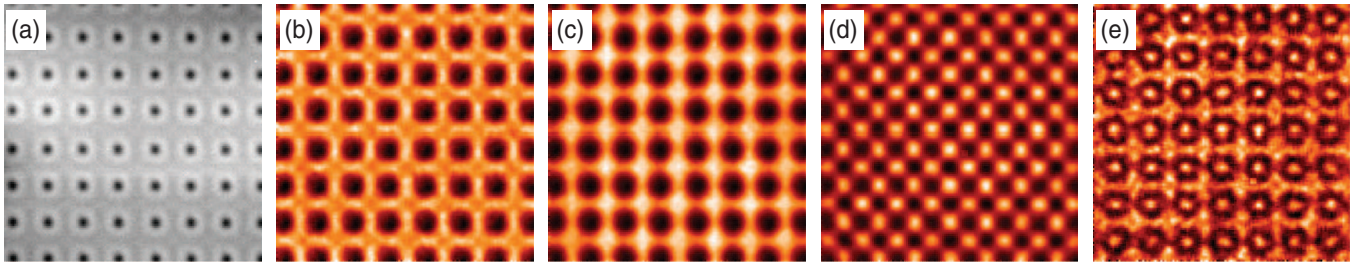

FIG. 21. Tunneling spectroscopy maps of the 9a × 5√3a (2.3 nm × 2.2 nm) CO grid structure. (a) STM topographic image. The grey color scale covers a height range of 530 pm. (b)–(e) Corresponding dI/dV maps at sample biases of −360 mV, −220 mV, −40 mV, and 420 mV, respectively. The color scale covers an impedance range from (b) 3.3 nS to 4.5 nS, (c) 2.4 nS to 4.0 nS, (d) 2.0 nS to 3.3 nS, and (e) 1.9 nS to 2.2 nS. See the supplementary material for a full series of dI/dV maps.[45] Image sizes 16 nm × 16 nm. Tunneling parameters, 1 nA, 500 mV. T = 4.3 K.

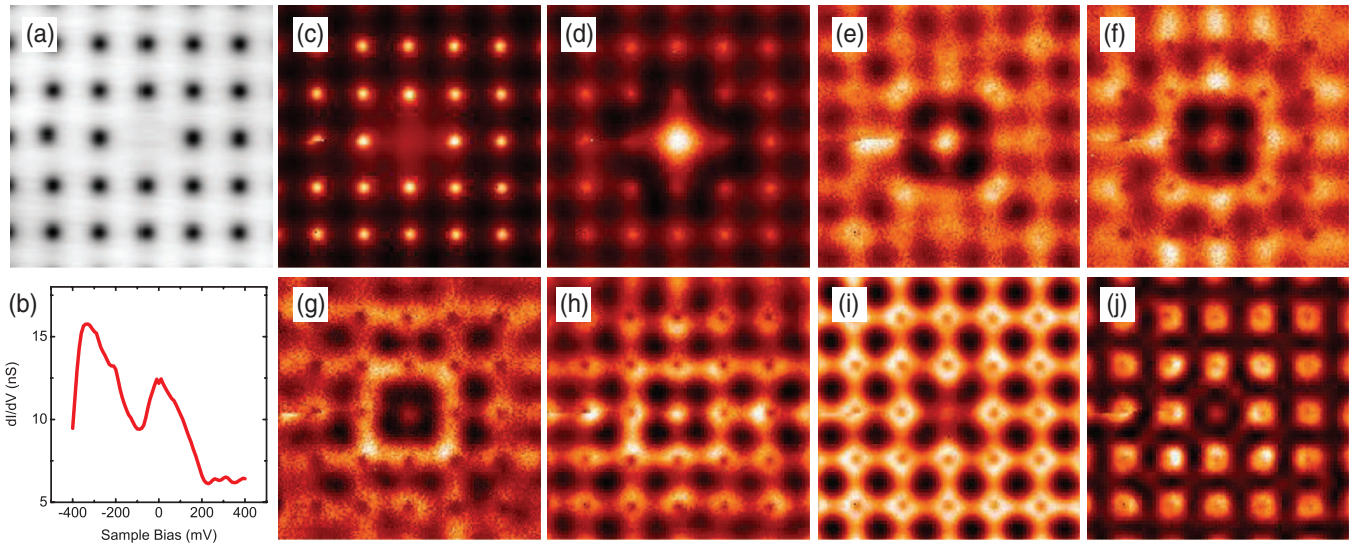

FIG. 22. Tunneling spectroscopy of a quantum dot formed from removing a single CO molecule from a 7a × 4√3a (1.79 nm × 1.77 nm) CO grid structure. (a) STM topography of CO grid. The grey color scale covers a height range of 750 pm. (b) dI/dV spectra from the center of the grid showing confined electronic states. (c)–(j) dI/dV maps obtained at sample biases, −400 mV, −320 mV, −240 mV, −200 mV, −30 mV, 0 mV, 100 mV, and 300 mV, respectively. Note the correspondence with the peaks in the spectrum in (b). The color scale covers an impedance range given in (b). See the supplementary material for a complete series of dI/dV maps. Tunneling parameters, 5 nA, −400 mV. T = 4.3 K.

construct artificial lattice grids and show that removing a single molecule from the lattice, i.e., creating a vacancy, results in a quantum dot with confined electronic states. By controlling the position of multiple vacancies, we demonstrate interacting quantum dots with quantum states showing bonding and anti-bonding wavefunction patterns.

Construction of nearly square artificial lattices on the hexagonal Cu(111) lattice requires a certain combination of lattice constants along the principal directions of the lattice. In this work, we consider nearly square lattices constructed with spacings $7a \times 4a\sqrt{3}$ and $9a \times 5a\sqrt{3}$, which correspond to 1.79 nm × 1.77 nm and 2.3 nm × 2.2 nm, respectively, with $a = 0.255$ nm being the nearest neighbor separation of the Cu(111) surface. Figures 20(a)–20(c) show the stages of construction of a $9a \times 5a\sqrt{3}$ lattice of CO molecules using the multi-pass planner, starting from a random deposition of CO molecules [Fig. 20(a)]. CO bonds to a top Cu site on the Cu(111) surface and appears as a depression in the STM images, resulting in a lattice of topographic minima [Fig. 20(c)].

In the construction of the simple nanostructures, we saw how the Cu(111) two-dimensional surface state electron band can be constrained to produce standing wave patterns. The standing wave patterns correspond to resonant quantum states. The Cu(111) surface state band is parabolic with a minimum at −437 meV below the Fermi-level.[44] In the case of the CO lattice in Fig. 20(c), each cell bounded by four CO molecules [Fig. 20(e)] acts as a confining barrier. Well-defined quantum confined electronic states can be seen in the differential conductance spectrum shown in Fig. 20(d). The peak intensities vary depending on whether the spectrum is taken in the center of the cell or in the bridge position between CO molecules. This reflects the change in nodal structure of the wavefunction probability for these states, which can be seen in the *dI/dV* line spectra taken along the vertical line in Fig. 20(e), which is shown as an image in Fig. 20(f). The arrows mark electronic states where the nodal structure oscillates as a function of energy. The full wavefunction probability across the two-dimensional lattice is shown in Fig. 21, which shows $dI/dV(\boldsymbol{r}, V_B)$ spatial maps across the grid at selected tunneling voltages, V_B. These tunneling voltages correspond to the values indicated by the arrows in Fig. 20(d). One can see that at −40 mV [Fig. 21(d)], the intensity is highest in the bridge positions. A full set of *dI/dV* maps can be seen in the supplementary material.[45]

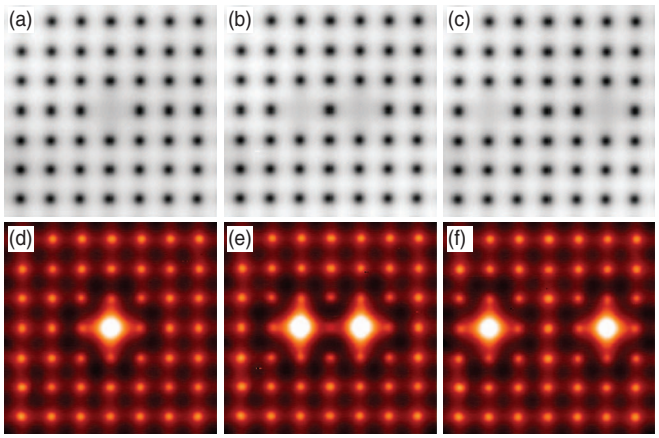

FIG. 23. Single and double quantum dots formed by removing CO molecules from the 7a × 4√3a (1.79 nm × 1.77 nm) CO grid structure. (a) STM image of a single QD with one CO molecule removed. (b) STM image of two QDs separated by one CO molecule with a separation of 3.6 nm. (c) STM image of two QDs separated by three CO molecules with a separation of 7.2 nm. The grey color scale covers a height range of 750 pm for (a), 850 pm for (b), and 870 pm for (c). (d)–(f) Corresponding closed loop *dI/dV* maps of the structures in (a)–(c) at an sample bias of −330 mV corresponding to a maximum in the tunneling spectrum (see Fig. 18). The two QDs in (b) are close enough to exhibit interaction with each as shown in Fig. 24. The color scale covers an impedance range from 13 nS to 20 nS. Tunneling set points from measurements, 5 nA, −330 mV. Images are 12.5 nm × 12.5 nm. T = 4.3 K.

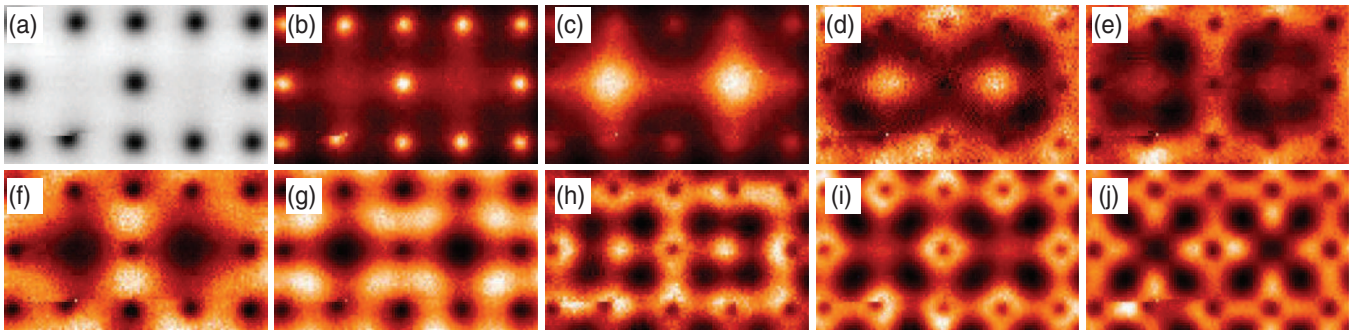

FIG. 24. Tunneling spectroscopy of two interacting quantum dots formed by removing two CO molecules from a 7a × 4√3a (1.79 nm × 1.77 nm) CO grid structure. (a) STM topographic image showing QDs spaced about 3.6 nm apart and separated by one CO molecule. The grey color scale covers a height range of 660 pm. (b)–(j) dI/dV maps at sample biases, −400 mV, −360 mV, −240 mV, −200 mV, −170 mV, −150 mV, 0 mV, 100 mV, and 200 mV, respectively. Note the asymmetries in maps (d)–(f) displaying bonding/anti-bonding character. The color scale covers a low to high impedance range from dark to bright. See the supplementary material for a complete series of dI/dV maps. STM image sizes 7.5 nm × 4.5 nm. Tunneling set points for measurements, 5 nA, −500 mV. T = 4.3 K.

Removal of a single CO molecule from the CO lattice creates a larger area for confinement and a stronger intensity in the confined quantum states, as shown in Fig. 22(b). The sequence of *dI/dV* maps shows the spatial profile for the two center localized states in Fig. 22(b) in maps at −320 mV [Fig. 22(d)] and at 0 mV [Fig. 22(h)]. More delocalized states forming pseudo-ring like patterns are seen at −200 mV [Fig. 22(f)] and −30 mV [Fig. 22(g)]. A full set of *dI/dV* spatial maps as a function of energy can be seen in the supplementary material.[45]

The potential of efficient single atom and molecule manipulation is demonstrated in Fig. 23, where we create multiple quantum dots and alter their coupling by varying the separation between the vacancies in the CO lattice. The three images in Figs. 23(a)–23(c) show a $7a \times 4a\sqrt{3}$ CO lattice with one vacancy, then two vacancies separated by $14a = 3.6$ nm, and $28a = 7.1$, respectively. The corresponding *dI/dV* maps [Figs. 23(d)–23(f)] show the lowest quantum state at −330 mV. We observe that at the large separation of 7.1 nm [Fig. 23(f)], the dots are not interacting and behave as isolated entities, whereas, at a separation of 3.6 nm [Fig. 23(e)] the quantum state shows some overlap in the region between the dots, indicating these dots are interacting. We examine the interaction in more detail in full spatial *dI/dV* maps as a function of energy, shown in Fig. 24 for the double vacancy in the $7a \times 4a\sqrt{3}$ CO lattice. Clear signs of interacting quantum dots are seen by the lack of reflection symmetry about the position the vacancies in the *dI/dV* maps. This is seen, for example, in the maps in Figs. 24(c)–24(f). Figures 24(d) and 24(e) demonstrate bonding and anti-bonding state character by the greater wavefunction probability in the central region of the two vacancies in Fig. 24(d), *vs*. diminished intensity in Fig. 24(e). A full set of *dI/dV* maps can be seen in the supplementary material.[45] These results demonstrate that quantum states can be tailor made with varying degrees of superposition.[30]

V. DISCUSSION AND FUTURE DIRECTIONS

We have developed a new method for the construction of nanostructures using atom manipulation with an autonomous atom assembly system and illustrated the technique through the construction of geometric confined nanostructures with single Co atoms and artificial lattice structures with CO molecules. We constructed more complex shapes over larger distances using a single region planning algorithm, which exhibited small atom placement errors due to piezo actuation nonlinearity. The use of multi-region planning was demonstrated to overcome these positioning limitations and autonomously produce atomically perfect nanostructures as requested, as shown in Figs. 18 and 19.

As a demonstration of the application of the AAA to molecular systems, we demonstrated the construction of artificial rectilinear lattices of CO molecules on the Cu(111) surface. We showed that a single CO vacancy in the lattice produced a quantum dot, with confined electronic states in the Cu(111) surface state band. Interacting quantum dots were produced by creating double vacancies with varying separations. Bonding and anti-bonding wavefunction probabilities can be observed in the *dI/dV* maps of the fabricated interacting quantum dots.

Future application of this technology could create a quantum toolkit which could readily produce tailored quantum states with application to, for example, quantum information processing and nanophotonics.

ACKNOWLEDGMENTS

We thank John Cugini, Alberto Lacaze, Steve Blankenship, and Allan Band for their contributions to this project, and we thank Mark Stiles for valuable discussions.

[1]J. A. Stroscio and W. J. Kaiser, *Scanning Tunneling Microscopy*, Methods of Experimental Physics Vol. 27 (Academic Press, 1993).
[2]R. Wiesendanger and H.-J. Guntherodt, *Scanning Tunneling Microscopy III: Theory of STM and Related Scanning Probe Methods* (Springer, Berlin, 1993).
[3]C. J. Chen, *Introduction to Scanning Tunneling Microscopy* (Oxford University Press, Oxford, 2008).
[4]S. Morita, F. J. Giessibl, and R. Wiesendanger, *Noncontact Atomic Force Microscopy* (Springer, Berlin, 2009), Vol. 2.
[5]D. M. Eigler and E. K. Schweizer, Nature (London) **344**, 524 (1990).
[6]J. A. Stroscio and D. M. Eigler, Science **254**, 1319 (1991).
[7]D. M. Eigler, C. P. Lutz, and W. E. Rudge, Nature (London) **352**, 600 (1991).

[8]M. F. Crommie, C. P. Lutz, and D. M. Eigler, Science **262**, 218 (1993).
[9]E. J. Heller, M. F. Crommie, C. P. Lutz, and D. M. Eigler, Nature (London) **369**, 464 (1994).
[10]G. Meyer, B. Neu, and K. H. Rieder, Phys. Status Solidi B-Basic Res. **192**, 313 (1995).
[11]G. Meyer, B. Neu, and K. Rieder, Appl. Phys. -Mater. Sci. Proc. **60**, 343 (1995).
[12]L. Bartels, G. Meyer, and K.-H. Rieder, Appl. Phys. Lett. **71**, 213 (1997).
[13]L. Bartels, G. Meyer, and K.-H. Rieder, Phys. Rev. Lett. **79**, 697 (1997).
[14]L. Bartels, G. Meyer, K.-H. Rieder, D. Velic, E. Knoesel, A. Hotzel, M. Wolf, and G. Ertl, Phys. Rev. Lett. **80**, 2004 (1998).
[15]S.-W. Hla, L. Bartels, G. Meyer, and K.-H. Rieder, Phys. Rev. Lett. **85**, 2777 (2000).
[16]H. C. Manoharan, C. P. Lutz, and D. M. Eigler, Nature (London) **403**, 512 (2000).
[17]J. Kliewer, R. Berndt, and S. Crampin, New J. Phys. **3**, 22 (2001).
[18]K.-F. Braun and K.-H. Rieder, Phys. Rev. Lett. **88**, 096801 (2002).
[19]A. J. Heinrich, C. P. Lutz, J. A. Gupta, and D. M. Eigler, Science **298**, 1381 (2002).
[20]N. Nilius, T. M. Wallis, and W. Ho, Science **297**, 1853 (2002).
[21]N. Nilius, T. M. Wallis, M. Persson, and W. Ho, Phys. Rev. Lett. **90**, 196103 (2003).
[22]G. V. Nazin, X. H. Qiu, and W. Ho, Phys. Rev. Lett. **90**, 216110 (2003).
[23]J. A. Stroscio and R. J. Celotta, Science **306**, 242 (2004).
[24]S. Fölsch, P. Hyldgaard, R. Koch, and K. H. Ploog, Phys. Rev. Lett. **92**, 056803 (2004).
[25]V. Iancu and S.-W. Hla, Proc. Natl. Acad. Sci. U.S.A. **103**, 13718 (2006).
[26]J. Lagoute, X. Liu, and S. Fölsch, Phys. Rev. B **74**, 125410 (2006).
[27]C. F. Hirjibehedin, C. P. Lutz, and A. J. Heinrich, Science **312**, 1021 (2006).
[28]C. F. Hirjibehedin, C.-Y. Lin, A. F. Otte, M. Ternes, C. P. Lutz, B. A. Jones, and A. J. Heinrich, Science **317**, 1199 (2007).
[29]M. Ternes, C. P. Lutz, C. F. Hirjibehedin, F. J. Giessibl, and A. J. Heinrich, Science **319**, 1066 (2008).
[30]C. R. Moon, C. P. Lutz, and H. C. Manoharan, Nat. Phys. **4**, 454 (2008).
[31]S. Fölsch, J. Yang, C. Nacci, and K. Kanisawa, Phys. Rev. Lett. **103**, 096104 (2009).
[32]S. Loth, M. Etzkorn, C. P. Lutz, D. M. Eigler, and A. J. Heinrich, Science **329**, 1628 (2010).
[33]A. A. Khajetoorians, J. Wiebe, B. Chilian, and R. Wiesendanger, Science **332**, 1062 (2011).
[34]K. K. Gomes, W. Mar, W. Ko, F. Guinea, and H. C. Manoharan, Nature (London) **483**, 306 (2012).
[35]S. Loth, S. Baumann, C. P. Lutz, D. M. Eigler, and A. J. Heinrich, Science **335**, 196 (2012).
[36]A. A. Khajetoorians, B. Baxevanis, C. Hübner, T. Schlenk, S. Krause, T. O. Wehling, S. Lounis, A. Lichtenstein, D. Pfannkuche, J. Wiebe, and R. Wiesendanger, Science **339**, 55 (2013).
[37]P. Löptien, L. Zhou, J. Wiebe, A. A. Khajetoorians, J. L. Mi, B. B. Iversen, P. Hofmann, and R. Wiesendanger, Phys. Rev. B **89**, 085401 (2014).
[38]J. A. Stroscio, E. W. Hudson, S. R. Blankenship, R. J. Celotta, and A. P. Fein, Proc. SPIE **4608**, 112 (2002).
[39]S. J. Russell and P. Norvig, *Artificial Intelligence: A Modern Approach* (Prentice Hall, Englewood Cliffs, NJ, 1995).
[40]E. W. Dijkstra, Numer. Math. **1**, 269 (1959).
[41]A. Balakirsky, *Framework for Planning with Incrementally Created Graphs in Attributed Problem Spaces* (IOS Press, Berlin, Germany, 2003).
[42]T. Hofmann, F. Pielmeier, and F. J. Giessibl, Phys. Rev. Lett. **112**, 066101 (2014).
[43]A. J. Weymouth, T. Hofmann, and F. J. Giessibl, Science **343**, 1120 (2014).
[44]A. Tamai, W. Meevasana, P. D. C. King, C. W. Nicholson, A. de la Torre, E. Rozbicki, and F. Baumberger, Phys. Rev. B **87**, 075113 (2013).
[45]See supplementary material at http://dx.doi.org/10.1063/1.4902536 for video files showing autonomous atom assemblies and STM dI/dV spectral maps as a function of tunneling energy.